Quasielastic light scattering of aqueous biliary lipid systems. Mixed micelle formation in bile salt-lecithin solutions

ARTICLE *in* BIOCHEMISTRY · MARCH 1980

Impact Factor: 3.02 · DOI: 10.1021/bi00545a001 · Source: PubMed

3 AUTHORS, INCLUDING:

Norm Mazer
Roche
101 PUBLICATIONS **6,537** CITATIONS
SEE PROFILE

Martin C Carey
Harvard University
213 PUBLICATIONS **12,216** CITATIONS
SEE PROFILE

Biochemistry

 Volume 19, Number 4 February 19, 1980

Quasielastic Light-Scattering Studies of Aqueous Biliary Lipid Systems. Mixed Micelle Formation in Bile Salt–Lecithin Solutions†

Norman A. Mazer,* George B. Benedek, and Martin C. Carey‡

ABSTRACT: From measurements of the autocorrelation function and time-averaged intensity of light scattered from aqueous bile salt–lecithin solutions, we deduced the mean hydrodynamic radius ($\bar{R}_h$), shape, and polydispersity of bile salt–lecithin mixed micelles as functions of bile salt species, lecithin to bile salt (L/BS) molar ratio, total lipid concentration (0.625–10 g/dL), temperature (20–60 °C), and NaCl concentration (0.15–0.6 M). Our data suggest that at low L/BS ratios (0 to ~0.6) simple bile salt micelles coexist in varying proportions with minimum-sized mixed micelles ($\bar{R}_h$, 18–35 Å). These solutions are highly polydisperse and display features dependent upon the particular bile salt species. At high L/BS ratios (>0.6), only mixed micelles are present, and their sizes increase markedly ($\bar{R}_h$, 20 → 300 Å) with increases in L/BS ratio and appear to diverge as the lecithin–bile salt phase limit is approached. The shape of the mixed micelles as deduced from light-scattering measurements and confirmed by transmission electron microscopy is disklike. The radii of the disks, however, are not compatible with Small's model of mixed micellar structure [Small, D. M. (1967a) *Gastroenterology 52*, 607] but are consistent with a new model proposed here in which bile salts and lecithin interact to form a *mixed bilayer* disk which is surrounded on its perimeter by bile salts. The inclusion of bile salts in a fixed stoichiometery within the interior of the bilayers is shown to provide a quantitative explanation for the divergence of the mixed micellar sizes, their temperature dependence, and the origin of the lecithin–bile salt phase limit. The influence of total lipid concentration on both mixed micellar size and the lecithin–bile salt phase limit is explained by the "mixed disk" model by taking account of the equilibrium between mixed micelles and bile salt monomers in the intermicellar solution. By use of this concept, deductions of the intermicellar bile salt concentration in taurocholate–lecithin solutions are made and are shown to vary as a function of mixed micellar size and temperature. The range of values obtained, 3–6 mM, is comparable in magnitude to the critical micellar concentration of the pure bile salt.

In contrast to synthetic short-chain (di-C6–C9) lecithins (1,2-diacyl-*sn*-glycero-3-phosphorylcholine) which form micellar aggregates in dilute aqueous solutions (Tausk et al., 1974), the biologically important long-chain lecithins (>di-C10) do not form micelles but rather form insoluble liquid crystalline bilayer structures when added to water (Small, 1967b). Bile salt molecules whose self-association properties were systematically investigated in an earlier study (Mazer et al., 1979) possess the remarkable ability to solubilize appreciable quantities of these lecithin bilayers by forming thermodynamically stable macromolecular aggregates known as mixed micelles (Carey & Small, 1970).

Based largely on results of X-ray diffraction studies of the hexagonal liquid crystalline phase in the bile salt–lecithin–water systems (Small & Bourgès, 1966), a molecular model for the structure of bile salt–lecithin mixed micelles was proposed (Small, 1967a). In this model, the mixed micelle consists of a disklike portion of a lecithin bilayer surrounded on its perimeter by bile salt molecules, oriented with their hydrophilic surfaces in contact with the aqueous solvent and their hydrophobic surfaces interacting with the paraffin chains of the lecithin molecules. This model rationalized how mixed micelles of two dissimilarly shaped molecules could furnish a completely hydrophilic surface to the aqueous solvent. An important quantitative aspect of this model, however, was its prediction of a linear increase in the radius of the mixed micellar disk with increases in the total lecithin–bile salt molar ratio (L/BS)[1] in solution (Shankland, 1970; Small, 1971).

† From the Department of Medicine, Harvard Medical School, Division of Gastroenterology, Peter Bent Brigham Hospital, Boston, Massachusetts 02115, and from the Department of Physics, Center for Materials Science and Engineering, Massachusetts Institute of Technology, Cambridge, Massachusetts 02138. *Received August 15, 1979.* Supported in part by National Institutes of Health Research Grants No. AM 18559 and AM 00195 (M.C.C.), National Science Foundation Grant DMR 7680895-A02 to the Center for Materials Science and Engineering, M.I.T., National Science Foundation Grant 7707666-CHE (G.B.B.), and grants from the Whitaker Health Sciences Fund.

* Correspondence should be addressed to this author at the Department of Medicine (Gastroenterology Division), Peter Bent Brigham Hospital, Boston, MA 02115. He is a former Insurance Medical Scientist Scholar sponsored by the Connecticut Mutual Life Insurance Co.

‡ Recipient of a Research Career Development Award (AM 00195) from the National Institutes of Health.

0006-2960/80/0419-0601$01.00/0

Although considered a major advance in our understanding of the physical chemistry of bile, this model and its quantitative predictions have never been adequately verified by direct measurements of micellar size, weight, or shape (Shankland, 1970). Moreover, the model suffers from a number of important conceptual problems. First, it does not explain how the transition from a pure bile salt solution containing globular or rod-shaped micelles (Mazer et al., 1979) to a bile salt–lecithin solution composed of disk-shaped structures is achieved. Second, the model provides little insight into the factors which limit the solubilization of lecithin in aqueous bile salt solutions and thus offers no explanation for the dependence of solubilizing capacity on temperature, bile salt species, NaCl concentration, and total lipid concentration (Carey & Small, 1978).

In an attempt to experimentally test the existing model of mixed micellar structure and to investigate the conceptual problems discussed above, we undertook a systematic investigation of mixed micelle formation in bile salt–lecithin solutions using the technique of quasielastic light-scattering spectroscopy (QLS). From our measurements of the autocorrelation function and mean intensity of the scattered light, we have determined the mean micellar size, shape, and polydispersity of these solutions as functions of the lecithin to bile salt ratio, bile salt species, total lipid concentration, temperature, and added NaCl concentration. To further support our deductions by the light-scattering technique, we have directly determined mixed micellar size and shape using transmission electron microscopy.

On the basis of our results, we propose a new model[2] for the molecular structure of bile salt–lecithin mixed micelles in which bile salts not only exist on the perimeter of lecithin bilayers but are also incorporated within their interior in high concentrations. In addition, the present work offers a quantitative interpretation of the micellar phase limit and also provides insights into the chemical equilibria between mixed micelles, simple micelles, and bile salt monomers.

Experimental Section

(*A*) *Materials.* Egg yolk lecithin (average M_r 775), which is similar in chain length distribution to biliary lecithin (Montet & Dervichian, 1971), was employed. The material was of grade I quality, obtained from Lipid Products, South Nuffield, Surrey, U.K., and was chromatographically pure (TLC) in a number of solvent systems. The sources and purity of the bile salts, NaCl, and water were identical with those described in our earlier study (Mazer et al., 1979).

(*B*) *Solutions.* Aqueous bile salt–lecithin solutions were prepared by the method of coprecipitation (Small et al., 1969; Carey & Small, 1978). After dissolving the appropriate amounts of each lipid in methanol or ethanol, the mixture was thoroughly dried under a stream of purified N_2 and then dried in vacuo (24–48 h), until a constant dry weight was obtained. The appropriate pure aqueous NaCl solvent was then added to give the desired total lipid concentration, and the solutions were then flushed with purified N_2, sealed, and equilibrated for at least 2 days at 4 °C with periodic vortex mixing. For specific studies, stock 10 g/dL (w/v) solutions were diluted with aqueous NaCl solvent with or without added bile salts to obtain lower total lipid concentrations, and these were likewise flushed with N_2 and equilibrated at 4 °C for at least 2 days. As taurine conjugated bile salts were the only species studied and as lecithin is zwitterionic between pH ≃2–12, no buffer was employed (Mazer et al., 1979) but the pH approximated 7.0 for all solutions.

(*C*) *Methods.* (*1*) *QLS Measurements.* QLS measurements were carried out exactly as described previously (Mazer et al., 1979). It should be noted, however, that in the case of mixed micellar solutions, the mean hydrodynamic radius, $\bar{R}_h$, and index of polydispersity, V, reflect not only the distribution of mixed micellar species but also contain contributions from any simple micelles which may coexist in solution. As in the studies of simple bile salt micelles, the autocorrelation functions obtained from mixed micellar solutions could generally be fit to a high degree of precision by using only two cumulants (Koppel, 1972). However, systems whose L/BS molar ratios were near the micellar phase limits were found to be considerably polydisperse and thus required a third cumulant to fit the time decay of the autocorrelation function. It is assumed that the $\bar{R}_h$ values derived in the present studies are in general unaffected by intermicellar interactions. This assumption is strongly supported by a number of previous experimental studies and theoretical arguments (Mazer et al., 1977, pp 359–381, 1979).

(*2*) *Time-Averaged Light Intensity Measurements.* Measurements of the time-averaged intensity, $\bar{I}$, of light scattered from bile salt–lecithin solutions were obtained as a function of temperature, L/BS molar ratio, and total lipid concentration as a means for deducing the shape of the mixed micelles (Mazer et al., 1976a, 1979). These $\bar{I}$ values were corrected for background scattering and normalized by an intensity standard whose absolute scattering intensity remained constant over the duration of the experiment. In this way, $\bar{I}$ values obtained on different samples could be compared directly with one another.

(*3*) *Transmission Electron Microscopy (TEM).* Samples for TEM were prepared at room temperature by conventional negative straining methods (Hall, 1953) using either 1% uranyl acetate or 1% phosphotungstic acid (PTA) buffer (pH 6). Samples were viewed on a Jelco electron microscope and photographed at ≃100 000× magnification.

Results

(*A*) *Mean Hydrodynamic Radii, $\bar{R}_h$.* (*1*) *Dependence on L/BS Molar Ratio, Bile Salt Species, and Temperature.* Parts A–D of Figure 1 show, respectively, the $\bar{R}_h$ values of 10 g/dL taurocholate–lecithin (TC–L), taurodeoxycholate–lecithin (TDC–L), tauroursodeoxycholate–lecithin (TUDC–L), and taurochenodeoxycholate–lecithin (TCDC–L) solutions in 0.15 M NaCl, as functions of L/BS molar ratio and temperature (20, 40, and 60 °C). At low L/BS ratios (0 to ~0.6), the behavior of $\bar{R}_h$ varies markedly between the different bile salt species, showing a small increase in TC–L and TUDC–L solutions, a significant decrease in TDC–L solutions, and a relatively constant behavior in TCDC–L solutions. The temperature dependence of $\bar{R}_h$ at these low ratios is similar to the temperature dependence in pure bile salt solutions (L/BS = 0). As will be discussed later, these species-dependent variations are consistent with a model in which simple bile salt micelles coexist in varying proportions with mixed micelles. In each figure we have, therefore, identified (by the horizontal arrows) the coexistence range for each bile salt species.[3] At

[1] Abbreviations used: QLS, quasielastic light-scattering spectroscopy; TC, taurocholate (3α,7α,12α-trihydroxy-5β-cholanoyltaurine); TDC, taurodeoxycholate (3α,12α-dihydroxy-5β-cholanoyltaurine); TCDC, taurochenodeoxycholate (3α,7α-dihydroxy-5β-cholanoyltaurine); TUDC, tauroursodeoxycholate (3α,7β-dihydroxy-5β-cholanoyltaurine); IMC, intermicellar bile salt concentration; L/BS, lecithin to bile salt molar ratio; TEM, transmission electron microscopy.

[2] This model was first proposed by Mazer et al. (1976b) and developed in more detail by Mazer et al. (1977, pp 383–402).

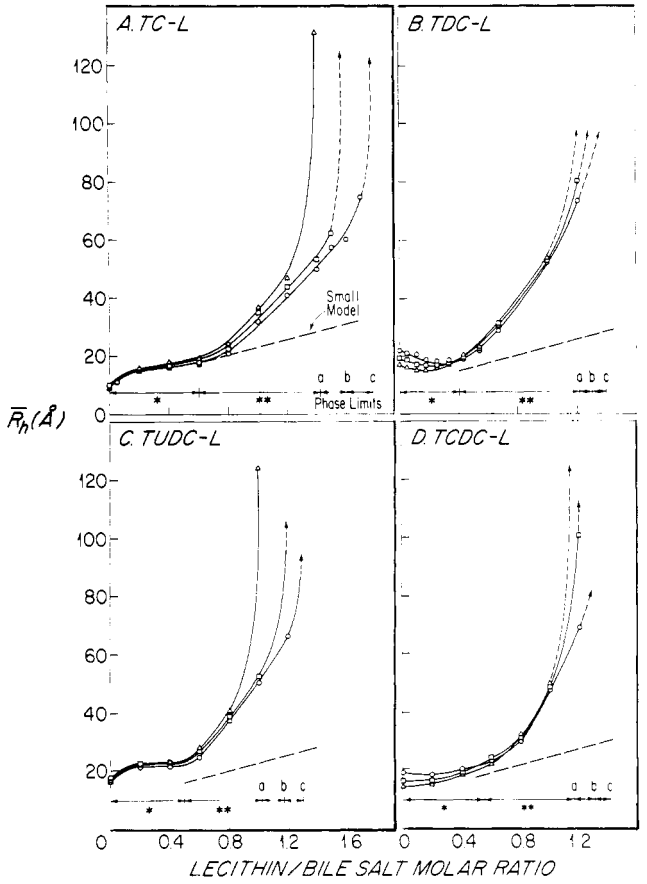

FIGURE 1: Mean micellar hydrodynamic radii, $\bar{R}_h$, in four bile salt–lecithin systems, plotted as a function of the lecithin/bile salt (L/BS) molar ratio at (○) 20, (□) 40, and (△) 60 °C; total lipid concentration was 10 g/dL; 0.15 M NaCl. At low L/BS ratios (*), systems contain simple *and* mixed micelles, whereas at high L/BS ratios (**), the systems contain only mixed micelles. The size of the mixed micelles appears to diverge at the L/BS ratio corresponding to the micellar phase limits appropriate to each temperature: (a) 60; (b) 40; (c) 20 °C. The dashed lines give the predictions of $\bar{R}_h$ based on Small's (1967a) model.

L/BS ratios greater than the upper limits of the coexistence ranges and below the mixed micellar phase limits (Carey & Small, 1978), the $\bar{R}_h$ values behave in a fashion which is independent of bile salt species. In these regimes, where we will show that only mixed micelles exist, the $\bar{R}_h$ values increase markedly as a function of L/BS ratio (from 20 Å to greater than 80 Å) and appear to diverge abruptly as the phase limits are approached. The temperature dependence of $\bar{R}_h$ at these high L/BS ratios is similar for the different bile species and opposite to that seen at low L/BS ratios (i.e., the mixed micellar sizes increase with elevation in temperature). This result is consistent with the effect of temperature elevation on the micellar phase boundaries which causes $\bar{R}_h$ to diverge at lower L/BS ratios.

Also shown in Figure 1A–D are dashed lines representing predictions of the $\bar{R}_h$ values based on Small's model of mixed micellar structure. At the beginning of the mixed micellar region, there is reasonable agreement between the Small model and the data. However, as the L/BS ratio increases, the experimental $\bar{R}_h$ values deviate markedly from the theoretical values, particularly as the phase limits are approached.

(*2*) *Dependence on Added NaCl Concentration.* Because of the strong influence of added NaCl on the size of the simple TDC micelles (Small, 1971; Mazer et al., 1979) and its effects on the bile salt–lecithin micellar phase limit (Carey & Small, 1978), an investigation of TDC–L solutions containing 0.6 M NaCl was conducted. Figure 2 displays the dependence of $\bar{R}_h$ on L/TDC ratio at 20, 40, and 60 °C. At low L/TDC ratios, the addition of lecithin causes a marked decrease in $\bar{R}_h$ (from ~60 to ~33 Å). As found in 0.15 M NaCl, the temperature dependence of $\bar{R}_h$ in this presumed coexistence regime of simple and mixed micelles parallels the strong temperature dependence at L/TDC = 0 (Mazer et al., 1979). Conversely for L/TDC ratios between 0.5 and the micellar phase limits, the $\bar{R}_h$ values increase markedly as a function of L/TDC (from ~33 Å to greater than 100 Å) and diverge as the phase limits are approached. In this regime, where only mixed micelles exist, the temperature dependence of $\bar{R}_h$ is opposite to that seen in low L/TDC ratios, again reflecting the fact that the micellar phase limits (which are about 12% smaller than in 0.15 NaCl) decrease with increases in temperature (Carey & Small, 1978).

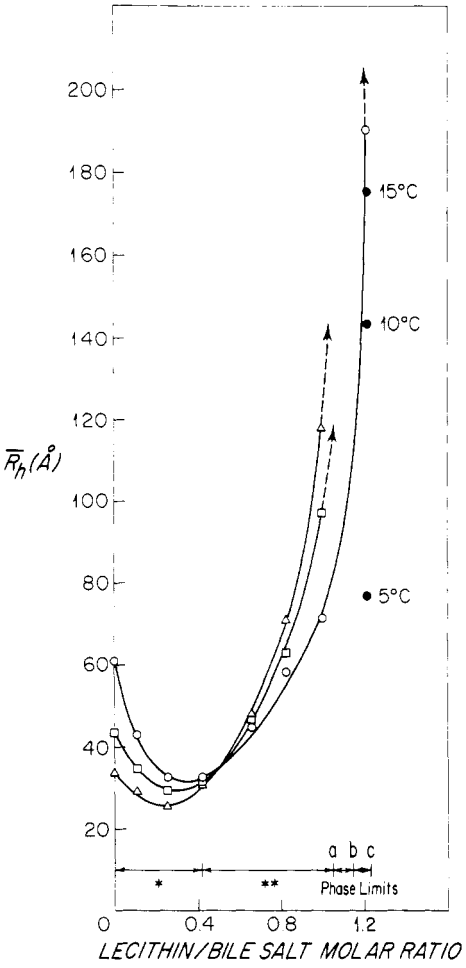

FIGURE 2: Dependence of mean hydrodynamic radii, $\bar{R}_h$, in 10 g/dL TDC–L solutions on the lecithin/bile salt (L/BS) molar ratio containing 0.6 M NaCl at (○) 20, (□) 40, and (△) 60 °C. Note that $\bar{R}_h$ initially decreases as a function of increasing L/BS ratio but then increases and appears to diverge at the micellar phase limits indicated by (a) 60 °C, (b) 40 °C, and (c) 20 °C. Simple and mixed micelles coexist at low L/BS ratios (*) and only mixed micelles are at high L/BS ratios (**). Also note the strong temperature dependence (5–20 °C) of $\bar{R}_h$ (●) at a fixed L/BS ratio of 1.2.

(*3*) *Dependence on Total Lipid Concentration.* As decreases in the total lipid concentration have been shown to markedly reduce the L/BS ratio at the micellar phase limit (Carey & Small, 1978), we therefore examined the influence of total lipid concentration on the $\bar{R}_h$ values of TC–L solutions. Parts A–C

[3] The upper limits for the coexistence region have been determined by inspection of the $\bar{R}_h$ data and correspond to the L/BS ratio prior to the marked upswing of the curves. The corresponding $\bar{R}_h$ values typically show little temperature dependence.

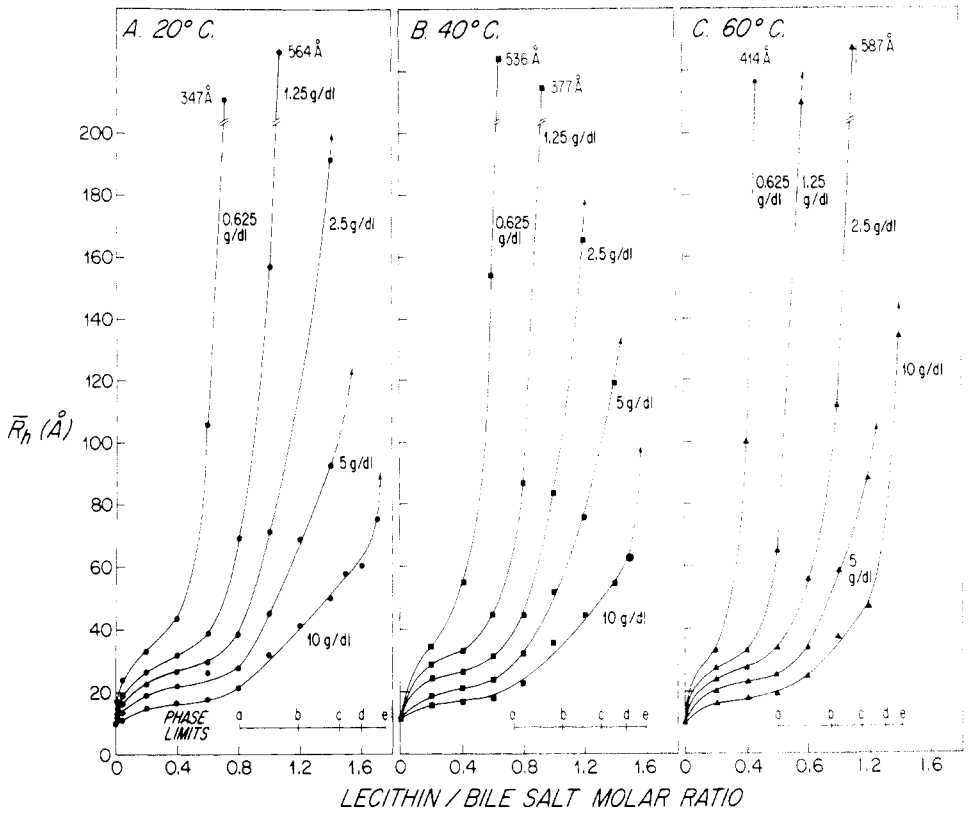

FIGURE 3: (A–C) Mean hydrodynamic radii, $\bar{R}_h$, of TC–L solutions at various total lipid concentrations (0.625–10 g/dL) and temperatures: (A) 20; (B) 40; (C) 60 °C. Note that $\bar{R}_h$ appears to diverge as the L/BS ratio approaches the micellar phase limits, which decrease with lowering of the total lipid concentration. The phase limits shown at the bottom of each panel represent the appropriate L/BS ratio for total lipid concentrations of (a) 0.625, (b) 1.25, (c) 2.5, (d) 5.0, and (e) 10.0 g/dL. $\bar{R}_h$ values indicated at the top of certain curves represent the size of bilayer vesicles formed in supersaturated systems at L/BS ratios of between 0.6 and 1.2.

of Figure 3 display $\bar{R}_h$ values as a function of L/TC ratio and total lipid concentration (0.625, 1.25, 2.5, 5, and 10 g/dL) at temperatures of 20, 40, and 60 °C, respectively. These data clearly show that with lowering of the total lipid concentration, the divergence in $\bar{R}_h$ occurs at lower L/TC ratios, in accordance with the reductions of the phase limits. Thus, at a fixed L/TC ratio, dilution of the total lipid concentrations with 0.15 M NaCl results in a dramatic increase in the $\bar{R}_h$ values. This unusual result is the opposite of what is seen in simple micellar systems (Mazer et al., 1976a, 1979) where decreases in lipid concentration produce decreases in micellar size. We will show later that the increase in $\bar{R}_h$ with dilution results from the equilibrium between bile salts in the mixed micelles and bile salts in the intermicellar solution. In fact, by taking account of this equilibrium, it is possible to abolish the increase in $\bar{R}_h$ that occurs upon dilution. This is accomplished by using a diluent that contains the appropriate intermicellar bile salt concentration, IMC, which is in equilibrium with the mixed micelles. Figure 4 demonstrates this effect for TC–L mixed micelles of two different sizes: $\bar{R}_h$ = 120 and 45 Å. The dashed curves show the dependence of $\bar{R}_h$ on total lipid concentration upon dilution with 0.15 M NaCl (as derived from Figure 3A). Under these conditions the L/TC ratio in each solution (L/TC = 0.65 for $\bar{R}_h$ = 120 Å and L/TC = 0.4 for $\bar{R}_h$ = 45 Å) remains constant. This large increase in $\bar{R}_h$ is abolished in the solid curves which are obtained by diluting the two systems with solvent that contains, respectively, 3.75 and 5.5 mM TC. The basis upon which these intermicellar bile salt concentrations were selected will be described later. Above the phase limits in Figure 3, the dilute TC–L solutions at equilibrium separate into two-phase systems containing a saturated micellar phase and a precipitated phase. QLS measurements on metastable supersaturated solutions (above

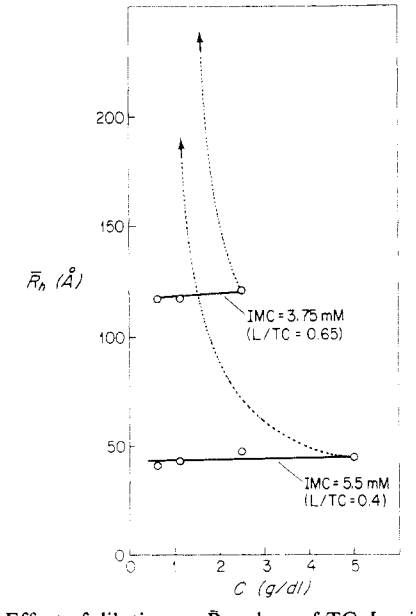

FIGURE 4: Effect of dilution on $\bar{R}_h$ values of TC–L mixed micelles at 20 °C in 0.15 M NaCl. Dotted curves represent the effect of diluting the total lipid concentration, C (g/dL), by using 0.15 M NaCl, as derived from the data of Figure 3A. Open circles show the preservation of micellar size when the systems are diluted with solvent containing the intermicellar bile salt concentrations, IMC, indicated on the figure.

the phase limit) suggest the presence of large bilayer vesicles (liposomes) which are relatively monodisperse ($\bar{V} \sim 20\%$) and have $\bar{R}_h$ values in excess of 400 Å.

(B) Deductions of Micellar Polydispersity. An analysis of solution polydispersity as measured by the variance parameter,

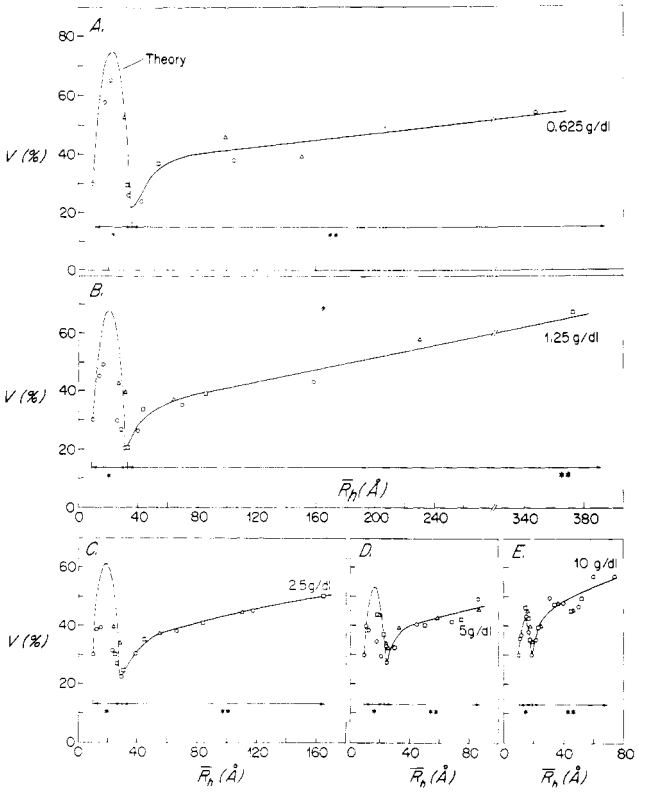

FIGURE 5: (A–E) Index of polydispersity, V, plotted vs. the corresponding $\bar{R}_h$ values measured in TC–L solutions at various temperatures [(○) 20; (□) 40; (△) 60 °C] and total lipid concentrations: (A) 0.625; (B) 1.25; (C) 2.5; (D) 5; (E) 10 g/dL. At low $\bar{R}_h$ values, simple and mixed micelles coexist, as shown by the horizontal arrows marked (*), and theoretical predictions (dashed curves) are shown for the dependence of V on $\bar{R}_h$ expected in these regions. At high $\bar{R}_h$ values, only mixed micelles are present as shown by the horizontal arrows marked (**). (See the text for further explanation.)

V, was carried out on TC–L solutions as functions of total lipid concentration, the L/TC ratio, and temperature. In Figure 5A–E, the V values for various L/TC ratios and temperatures (20–60 °C) are plotted vs. the corresponding $\bar{R}_h$ values for each of five total lipid concentrations. In each case, a single curve fits within experimental error the dependence of V on $\bar{R}_h$. Although numerically different, the five curves are qualitatively similar. At low $\bar{R}_h$ values (i.e., solutions with low L/TC ratios) the V values rise and then fall on a narrow peak whose height and width depend on the total lipid concentration. Our subsequent theoretical analysis will show that these peaks are quantitatively consistent with the polydispersity expected from the coexistence of both simple TC micelles ($\bar{R}_h$ = 10 Å) and mixed micelles whose $\bar{R}_h$ values correspond to the $\bar{R}_h$ values at the right base of the peaks. These plots demonstrate that the size of the minimum mixed micelles increases from ~18 Å at 10 g/dL to ~35 Å at 0.625 g/dL. For larger $\bar{R}_h$ values, the V values represent the breadth of the distribution of the mixed micellar species. In these regimes the five curves are also similar, showing an initial rise from minimum V values of 20–30%, followed by a slow increase as a function of $\bar{R}_h$ (to V values between 50 and 70%). The latter values which are attained at $\bar{R}_h$ > 100 Å indicate that the size distributions corresponding to the large mixed micelles are exceedingly broad. In fact, in one such solution (1.25 g/dL; L/TC = 1.0; T = 40 °C), an approximate representation of the size distribution of mixed micellar sizes was obtained. This solution gave an $\bar{R}_h$ of 377 Å and V = 67%, and, from the third cumulant, the skewness, S, of the distribution (Mazer, 1973) was estimated at 86%. From these three parameters, a bar graph

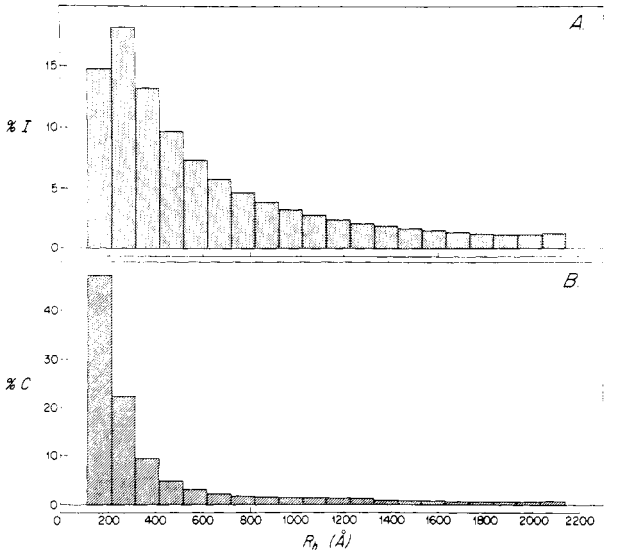

FIGURE 6: (A and B) Representations of the distribution of mixed micellar sizes in a TC–L solution (1.25 g/dL; L/TC = 1.0; T = 40 °C), as derived from Pearsonian analysis (see the text). In (A), the relative scattered intensity, % I, is plotted vs. the hydrodynamic radii (R_h) of the mixed micelles. In (B), the relative concentrations (w/v), as a percentage of total concentration (% C), are plotted vs. the R_h values.

representation of the micellar size distribution was derived by using the Pearsonian system of frequency curves (Mazer, 1973; Cohen et al., 1976). This representation (Figure 6A) plots % I, the percent of the total light intensity scattered by mixed micelles, as a function of their individual hydrodynamic radii, R_h. The R_h values range from ~100 to ~2100 Å, and a major portion of the scattered intensity is produced by mixed micelles with R_h values less than 1000 Å. The % I values given in Figure 6A in turn can be used to deduce the relative concentrations (w/v) of the mixed micelles as a function of R_h. However, such deductions require knowledge of the mixed micellar shape, given in the next section. Anticipating these results, we plot in Figure 6B % C, the percent of the total mixed micellar concentration (w/v) corresponding to mixed micelles with a hydrodynamic radius, R_h. This shows that mixed micelles with R_h values less than 400 Å comprise the greatest fraction of the total lipid concentration.

(*C*) *Deduction of Mixed Micellar Shape.* In earlier studies (Mazer et al., 1976a, 1979), we have deduced micellar shape from a quantitative analysis of the dependence of $\bar{I}$ (the time-averaged scattered light intensity) on $\bar{R}_h$ where both parameters were measured as functions of temperature. In the present study, we generalize this approach to utilize $\bar{I}$ and $\bar{R}_h$ values obtained in various TC–L mixed micellar solutions as functions of temperature, L/TC molar ratio, and total lipid concentration. By treating the mixed micellar solutions as monodisperse and noninteracting (Mazer et al., 1976a), $\bar{I}$ is given by

$$\bar{I} = ACMP \qquad (1)$$

where A is a calibration constant (depending on n, the index of refraction of the solution, and dn/dc, the refractive index increment), C is the concentration (w/v) of mixed micelles [equal to the total lipid concentration minus the intermicellar concentration (IMC) of bile salt monomers], M is the micellar weight, and P is the scattering form factor (Kerker, 1969) which describes the angular anisotropy of the scattered light. Neglecting the very weak influences of temperature, total lipid concentration, and L/TC ratio on the value of A, it follows that the quantity $\bar{I}/C$ will be proportional to the product MP

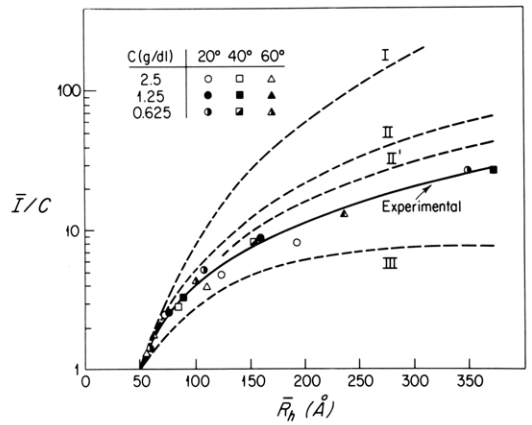

FIGURE 7: Experimental and theoretical dependence of the reduced intensity ($\bar{I}/C$) on the mean hydrodynamic radius, $\bar{R}_h$, of the micelles. Data are derived from a total lipid concentration of 0.625–2.5 g/dL at 20, 40, and 60 °C (see the key). Theoretical curves represent different mixed micellar shapes: I, monodisperse spheres; II, monodisperse disks (thickness 50 Å); III, monodisperse rods (diameter 50 Å). Curve II′ represents calculations for polydisperse disks (Appendix B) and is in closest agreement with the experimental data (solid line).

independent of the conditions under which $\bar{I}$ is measured. For a given value of $\bar{R}_h$, one can show that the corresponding product MP will have different values depending on the micellar shape. For this reason, a deduction of micellar shape can be made experimentally by analyzing the dependence of $\bar{I}/C$ (equivalent to MP) on $\bar{R}_h$. In Figure 7, experimental values of $\bar{I}/C$ are plotted vs. the corresponding $\bar{R}_h$ by using data obtained from dilute TC–L solutions (0.625–2.5 g/dL) at temperatures and L/TC ratios where only large mixed micelles are present ($50 < \bar{R}_h < 400$ Å). To within experimental error (±10%), these points fall on a single curve representing the experimental dependence of $\bar{I}/C$ on $\bar{R}_h$. In addition to this experimental curve, we have also plotted in Figure 7 the theoretical curve of the dependence of MP on $\bar{R}_h$ assuming that the micelles are as follows: I, monodisperse spheres; II, monodisperse disks (thickness 50 Å); III, monodisperse rods (diameter 50 Å). [The rationale for choosing these dimensions is given in Mazer (1978).] Because of the arbitrary calibration constant A, all curves (experimental and theoretical) have been normalized to unity at $\bar{R}_h = 50$ Å to allow for a comparison between theory and experiment which involves no free parameters. The equations for calculating the hydrodynamic radii, molecular weight, and form factors for rods, disks, and spheres are given in Appendix A. Comparing theory with experiment, one finds that the experimental dependence lies between the curves for disks (II) and rods (III); however, the experimental data is in closer agreement with the "disk" curve. One possible source for this discrepancy is the neglect of the appreciable polydispersity found in the mixed micellar solutions, particularly when $\bar{R}_h$ is large. To correct the theoretical curves for the effects of polydispersity, one must calculate a "weight average" of MP ($\sum C_i M_i P_i / \sum C_i$) using the micellar size distribution associated with each value of $\bar{R}_h$. Curve II′ is an attempt to incorporate in an approximate way (see Appendix B) the experimentally measured degrees of polydispersity into a theoretical curve which assumes a disklike micellar shape. By virtue of the downward shifting of the disk curve, the agreement between theory and experiment is much improved. When similar corrections are applied to curves I and III, the data further disagrees with the rodlike shape and only slightly improves with the case of the spherical shape. Thus, although the $\bar{R}_h$ values are inconsistent with the sizes of the disks predicted by Small's model, they are consistent

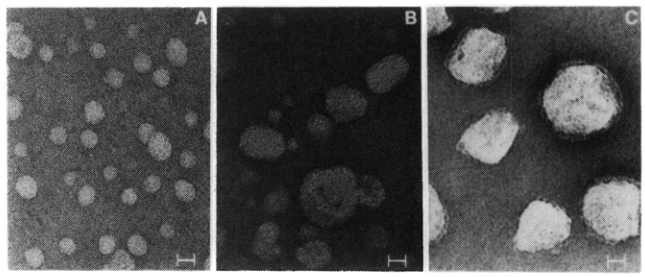

FIGURE 8: (A–C) Transmission electron micrographs of bile salt–lecithin mixed micelles negatively stained with 1% uranyl acetate (A and B) and 1% phosphotungstic acid (C), respectively. In plates A and B the micelles in a taurocholate–lecithin solution of L/TC ratio 0.42 (total lipid concentration 1 g/dL) and 0.85 (total lipid concentration 0.78 g/dL) are shown. In plate C, the micelles in a taurochenodeoxycholate–lecithin solution (L/TCDC = 1.0; total lipid concentration 0.32 g/dL) are shown. Note the increase in the radii of the mixed micelles from ~100 to 400 Å as the L/BS ratio increases when compared with the 200-Å scale (—) at the bottom. (See Table I for the corresponding $\bar{R}_h$ values.)

Table I: Comparison of Micellar Radii from Quasielastic Light-Scattering Spectroscopy and Transmission Electron Microscopy

plate	$\bar{R}_h$[a] (Å)	V[b] (%)	r^{QLS}[c] (Å)	r^{EM}[d] (Å)
Ia (TC–L)	35	32	45	80–100
Ib (TC–L)	200	70	250	160–360
Ic (TCDC–L)	380	80	500	350–400

[a] Observed mean hydrodynamic radius. [b] Variance, an index of micellar polydispersity. [c] Mean disk radius derived from $\bar{R}_h$ values. [d] Range of disk radii from examination of the photomicrographs.

with a disk shape whose thickness is comparable to a lecithin bilayer.

(*D*) *Electron Microscopy of Bile Salt–Lecithin Solutions.* Transmission electron microscopy was performed on dilute TC–L and TCDC–L solutions (<1 g/dL) as a function of the L/BS molar ratio in order to investigate samples with different $\bar{R}_h$ values. Parts A, B, and C of Figure 8 show electron photomicrographs of the mixed micelles seen in three solutions with $\bar{R}_h$ values measured at 35, 200, and 380 Å, respectively. It is evident that the particles shown in these photographs are approximately disk-shaped with a range of radii that increases in accordance with the $\bar{R}_h$ values, as tabulated in Table I. Although there is not precise agreement between the TEM radii, r^{EM}, and the disk radii, r^{QLS}, estimated from the $\bar{R}_h$ values, there is, nevertheless, a good correlation between the two sets of numbers. In view of this, we feel confident that the particles shown are not artifacts of the sample preparation and that they indeed support our previous deduction that the mixed micelles are disk-shaped.

Discussion

(*A*) *Overview: Phase Diagram of the Micellar Zone in Aqueous Bile Salt–Lecithin Solutions.* As noted previously, the dependence of $\bar{R}_h$ on the L/BS ratio qualitatively suggests the existence of two distinct regimes of micellar behavior in bile salt–lecithin systems. At low L/BS ratios, simple bile salt micelles appear to coexist with a minimum sized mixed micelle containing bile salt and lecithin. As the lecithin content of these solutions increases, the population of simple micelles decreases in order to furnish the bile salt molecules needed to form the mixed micelles. Finally, a critical L/BS ratio is reached [denoted by $(L/BS)_{coexistence}$] at which the solution contains only minimum mixed micelles in equilibrium with a population of bile salt monomers. Above this ratio the solu-

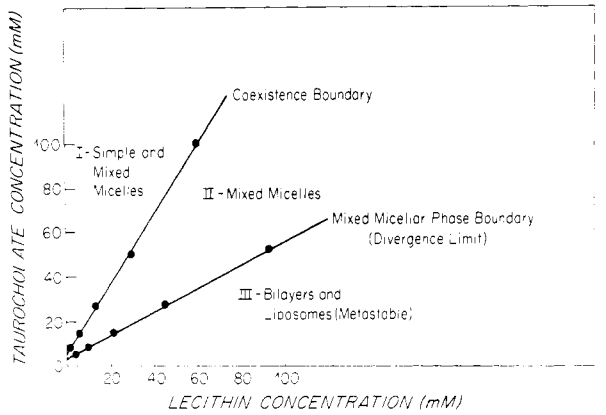

FIGURE 9: Phase diagram for taurocholate–lecithin system at 20 °C. Region I corresponds to concentrations at which simple and mixed micelles coexist. In region II only mixed micelles are present, and in region III insoluble bilayers and metastable liposomes are formed.

bilization of further lecithin necessitates a reorganization of mixed micellar size and structure. Our data suggest that the mixed micelles are disk-shaped, with radii that increase nonlinearly with L/BS ratio and appear to diverge at the L/BS ratio corresponding to the mixed micellar phase limit, $(L/BS)_{\text{phase limit}}$. Above this ratio the system can solubilize no additional lecithin and consists of precipitated bilayer structures. Under certain conditions, such supersaturated solutions may exist in a metastable state of relatively monodisperse bilayer vesicles prior to precipitation (Mazer, 1978).

From inspection of the $\bar{R}_h$ data given in Figure 3, we have determined values for $(L/BS)_{\text{coexistence}}$ and $(L/BS)_{\text{phase limit}}$ as functions of the total lipid concentration (0.625–10 g/dL). Using these values, we have derived a phase diagram characterizing the micellar zone of the TC–L system at 20 °C. This is shown in Figure 9 where the coordinate axes correspond to the concentrations of TC (mM) and lecithin (mM), respectively. The diagram consists of three regions separated by two boundaries. The coexistence boundary separates region I, where both simple and mixed micelles exist, from region II, where only mixed micelles are present. The micellar phase limit boundary (where $\bar{R}_h$ is diverging) separates region II from region III, where bilayers and metastable vesicles are formed. The fact that both boundaries are straight lines (to within experimental error) will be interpreted in the following sections, where a detailed quantitative analysis of the $\bar{R}_h$ data obtained in regions I and II is given. In this discussion it will be shown that the principle of material conservation used in conjunction with a minimum number of ad hoc assumptions concerning the structure and equilibrium of bile salt–lecithin mixed micelles can provide a simple theoretical understanding of mixed micelle formation.

(B) Analysis of Region I: Coexistence of Simple and Mixed Micelles. That simple and mixed micelles coexist at low L/BS ratios has already been qualitatively supported by the fact that the $\bar{R}_h$ values obtained with different bile salt species at low L/BS ratios have a magnitude and temperature-dependence characteristic of the particular species (Mazer et al., 1979). That this is not simply the result of a swelling of the simple micelles by the addition of lecithin molecules is evident from the observation that the $\bar{R}_h$ values of TDC–L solutions actually decrease as the L/BS ratios first increase. Quantitiative support for the coexistence model is provided by the following theoretical analysis of the $\bar{R}_h$ and V values obtained in TC–L and TDC–L solutions.

We assume that for L/BS molar ratios between 0 and $(L/BS)_{\text{coexistence}}$, the system contains simple micelles of mean hydrodynamic radius $\bar{R}_s$ coexisting with mixed micelles of mean hydrodynamic radius $\bar{R}_m$. In such a system, the overall mean hydrodynamic radius will be given by

$$\frac{1}{\bar{R}_h} = \frac{\bar{R}_s^{-1} + (I_m/I_s)\bar{R}_m^{-1}}{1 + I_m/I_s} \tag{2}$$

where I_m/I_s is the ratio of intensities scattered by the mixed micelles and simple micelles, which will depend on their relative concentrations (w/v) C_m and C_s and micellar weights $\bar{M}_m$ and $\bar{M}_s$:

$$\frac{I_m}{I_s} = C_m\bar{M}_m/(C_s\bar{M}_s) \tag{3}$$

To calculate $\bar{R}_h$ for L/BS ratios between 0 and $(L/BS)_{\text{coexistence}}$, the ratio C_m/C_s must be determined as a function of L/BS. To do this we assume that each mixed micelle in the coexistence regime contains lecithin and bile salt molecules in a molar ratio denoted by the parameter γ. Thus, if a solution contains C_{BS} bile salts (mM) and C_L lecithins (mM) [where $C_L/C_{BS} \leq (L/BS)_{\text{coexistence}}$], there will be $\gamma^{-1}C_L$ bile salts present in the mixed micelles. Allowing for a small intermicellar concentration of bile salt monomers, IMC, there will remain $C_{BS} - \gamma^{-1}C_L - \text{IMC}$ bile salts available to form simple micelles. It follows that the weight concentrations C_s and C_m will be given by

$$C_s = M_{BS}(C_{BS} - \gamma^{-1}C_L - \text{IMC})$$

$$C_m = M_L C_L + M_{BS}\gamma^{-1}C_L \tag{4}$$

where M_{BS} and M_L are the molecular weights of a bile salt and lecithin molecule, respectively. The ratio C_m/C_s is therefore

$$\frac{C_m}{C_s} = \left(\frac{M_L}{M_{BS}} + \gamma^{-1}\right)\frac{C_L}{C_{BS} - \gamma^{-1}C_L - \text{IMC}} \tag{5a}$$

$$= \left(\frac{M_L}{M_{BS}} + \gamma^{-1}\right)\frac{C_L/C_{BS}}{1 - (\gamma^{-1}C_L/C_{BS} + \text{IMC}/C_{BS})} \tag{5b}$$

From eq 5b it is apparent that the coexistence limit will be reached ($C_m/C_s \to \infty$) when the L/BS ratio (i.e., C_L/C_{BS}) is given by

$$(L/BS)_{\text{coexistence}} = \gamma\left(1 - \frac{\text{IMC}}{C_{BS}}\right) \tag{6}$$

Alternatively, the set of concentrations C_{BS} and C_L corresponding to the coexistence limit at various total lipid concentrations should satisfy the linear relationship

$$C_{BS} = \gamma^{-1}C_L + \text{IMC} \tag{7}$$

Figure 9 does in fact demonstrate that the experimentally deduced TC and lecithin concentrations corresponding to the coexistence limits do indeed satisfy eq 7. Furthermore, from the slope and intercept of the coexistence boundary, we obtain values for γ of 0.65 and IMC of 6 mM. Now, using these values of γ and IMC in eq 5, one can calculate C_m/C_s as a function of the L/BS ratio for various total lipid concentrations. Combining this with the values of $\bar{R}_s$ and $\bar{R}_m$ obtained by inspection of the $\bar{R}_h$ data of Figure 3 and estimates of the ratio $\bar{M}_m/\bar{M}_s$ which is deduced experimentally from the scattered intensities,[4] one can employ eq 2 and 3 to calculate

Table II: Parameters Used in the Calculation of the Coexistence Theory in TC-L Solutions

C (g/dL)[a]	$\bar{R}_s$[b] (Å)	$\bar{R}_m$[c] (Å)	$(L/BS)_{coexistence}$[d]	$\bar{M}_m/\bar{M}_s$[e]	V_s[f] (%)	V_m[g] (%)
10	10	18	0.6	4.5	30	30
5	10	23.5	0.6	9.0	30	28
2.5	10	27.5	0.5	11.5	30	23
1.25	10	31.5	0.4	16.0	30	20
0.625	10	35	0.25	19.0	30	22

[a] Total lipid concentration. [b] Mean hydrodynamic radius of simple micelles. [c] Mean hydrodynamic radius of minimum-sized mixed micelles. [d] Lecithin/bile salt molar ratio at the upper limit of the coexistence range. [e] Ratio of mixed micellar weights to simple micellar weight. [f] Variance of simple micellar sizes. [g] Variance of mixed micellar sizes.

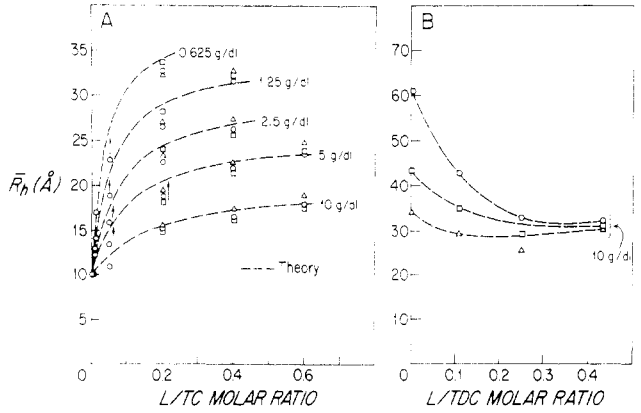

FIGURE 10: (A and B) Comparison of theoretical with experimental $\bar{R}_h$ (Å) data for (A) TC–L solutions in 0.15 M NaCl at various total lipid concentrations (0.625–10 g/dL) and (B) TDC–L solutions in 0.6 M NaCl at one total lipid concentration (10 g/dL). The dashed theoretical curves are derived on the assumption of the coexistence of simple and mixed micelles at low L/BS ratios. In (A) a single curve appropriate to each concentration is seen to fit the $\bar{R}_h$ values measured at three temperatures [(○) 20; (□) 40; (△) 60 °C], whereas in (B) a different theoretical curve is needed at each temperature. (See the text for details.)

$\bar{R}_h$ as a function of L/BS ratio in the coexistence regime (region I). Figure 10A shows a comparison between theory and experiment for the five total lipid concentration studies in the TC–L system. The experimental parameters used in these calculations are given in Table II. At each concentration, the theoretical curves are seen to be in reasonably good agreement with the experimental $\bar{R}_h$ values obtained at 20, 40, and 60 °C. The knee-shaped dependence of $\bar{R}_h$ on L/BS ratios in this system is thus numerically consistent with the coexistence of simple and mixed micelles. The fact that the size of the minimum mixed micelle $\bar{R}_m$ has an apparent dependence on total lipid concentration (Table II) is not explained by the present model. It may be due to an anomalous influence of intermicellar interactions on the diffusion coefficients measured at high total lipid concentrations, an effect which is assumed to be neglible in our deduction of $\bar{R}_h$. Alternatively, the growth of $\bar{R}_m$ with dilution may represent a real effect whose explanation involves a more complex model of the chemical equilibria involved in the coexistence region.

A further application of the coexistence model is in predicting the dependence of the V values on $\bar{R}_h$ in region I where $\bar{R}_s \leq \bar{R}_h \leq \bar{R}_m$. As shown in Appendix C, the V value can be calculated from the variance of the distribution of simple micelles V_s, the variance of the "minimum" mixed micelles V_m, the micellar sizes $\bar{R}_s$ and $\bar{R}_m$, and the ratio I_m/I_s. Since the values of V_s and V_m are also taken from experiment (see Table II), the prediction of V as a function of $\bar{R}_h$ likewise involves no free parameters. As seen in Figure 5, the coexistence theory predicts that the V values should attain maxima at $\bar{R}_h$ values that are midway between $\bar{R}_s$ and $\bar{R}_m$. These variance "peaks" are precisely what is found experimentally, again adding strong support for the model and also demonstrating that the specific polydispersity that occurs in the coexistence region can be sizable.

As final evidence in support of the coexistence model, we analyze the dependence of $\bar{R}_h$ on the L/TDC ratio measured in 0.6 M NaCl. As seen in Figure 2, the $\bar{R}_h$ values in this system decrease dramatically as the L/TDC ratio increases. Qualitatively, this occurs for two reasons. The first is that the minimum mixed micelle ($\bar{R}_m \simeq 31.5$ Å) is considerably smaller than the large rod-shaped simple micelles which form in 0.6 M NaCl. The second is that as the concentration of simple micelles, C_s, decreases, so does the mean hydrodynamic radius of the simple micelles, $\bar{R}_s$, in accordance with the model of primary–secondary micelle equilibrium developed in the preceding paper (Mazer et al., 1979). Because $\bar{R}_s$ is no longer a constant in the TDC–L solutions, the equations for calculating $\bar{R}_h$ are somewhat more complicated than those in the case of the TC–L solutions. Nevertheless, the prediction of $\bar{R}_h$ vs. L/TDC ratio can be performed by using parameters derived entirely from experiment (see Appendix D). In Figure 10B, we compare theoretical predictions of $\bar{R}_h$ derived at 20, 40, and 60 °C with the experimental values. At 20 °C, the predicted curve is in excellent agreement with experiment, whereas at 40 and 60 °C, the predicted curves do not reach minima quite as deep as the experimental values. Nevertheless, the general character of the theoretical curves closely resembles the experimental points and thus offers good support for the model.

(*C*) *Region II: A New Model for the Structure of the Bile Salt–Lecithin Mixed Micelle.* Although our $\bar{R}_h$ results are inconsistent with the predictions of Small's model, it is useful nevertheless to first give a brief description of the qualitative and quantitative aspects of this model. As shown in Figure 11A, the Small model of the mixed micelle consists of a lecithin bilayer disk surrounded on its perimeter by bile salts oriented so that their hydrophilic surfaces face the aqueous solution, while their hydrophobic surfaces interact with the hydrocarbon chains of the lecithin. The following geometric considerations imply that the radius, r, of the bilayer disk must increase linearly with the ratio of lecithin to bile salt molecules in the mixed micelle. If σ represents the number of lecithin molecules per unit area in the bilayer and ρ represents the number of bile salts per unit length of the disk's perimeter, then n_L, the number of lecithin molecules in a mixed micelle of radius r, will be equal to $\pi r^2\sigma$ whereas n_{BS}, the number of bile salt molecules, will equal $2\pi r\rho$. Solving for r, one obtains the linear dependence

$$r = \frac{2\rho}{\sigma}\frac{n_L}{n_{BS}} \qquad (8)$$

[4] At constant total lipid concentration the ratio $\bar{M}_m/\bar{M}_s$ should equal the ratio of the scattered intensities obtained at $(L/BS)_{coexistence}$ and L/BS = 0, respectively (see eq 1). Such data were employed to obtain the values given in Table II.

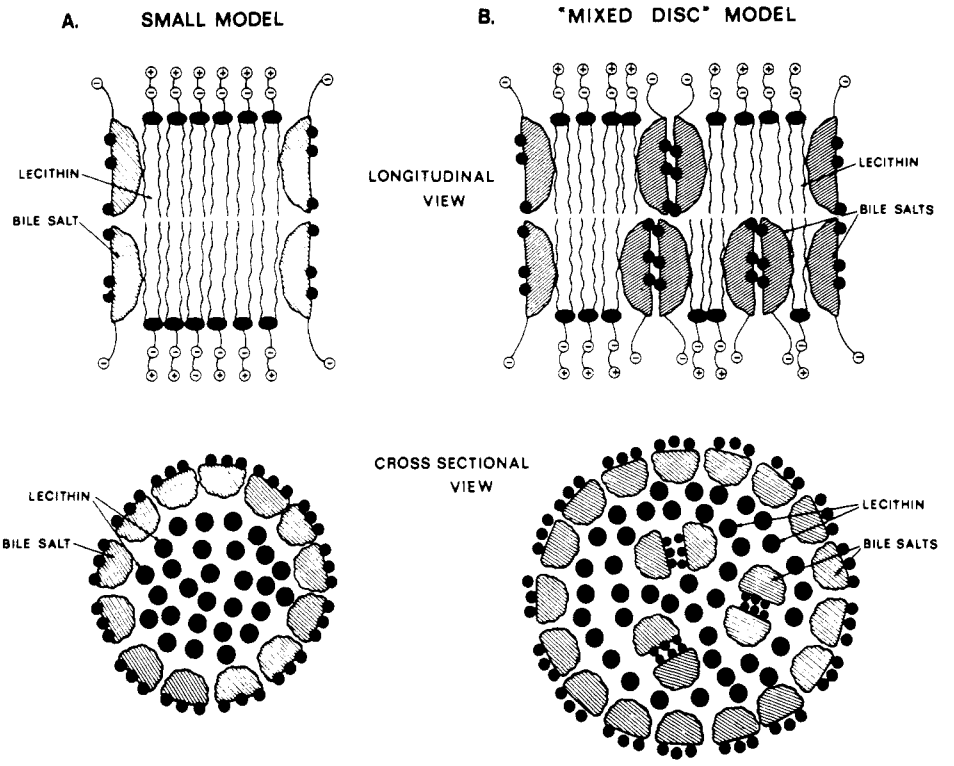

FIGURE 11: (A and B) Schematic models for the structure of the bile salt–lecithin mixed micelle, shown in longitudinal (cut through the disk diameter) and cross section (cut through middle of the hydrocarbon steroid parts and fatty acid chains of bile salts and lecithins, respectively). The closed circles and ovals represent the nonionic polar groups of the molecules, and the open circles with negative and positive signs represent the ionic polar parts of the molecules. Small's mixed micellar model is shown in Figure 11A. Our mixed disk model is shown in Figure 11B. Note that hydrogen-bonded bile salts are incorporated within the interior of the bilayer in the mixed disk model.

Experimentally, variations in the ratio n_L/n_{BS} are induced by changing the molar concentrations of lecithin, C_L, and bile salt, C_{BS}, present in the mixed micellar solution. Assuming the mixed micelles to be monodisperse,[5] it follows that n_L/n_{BS} will be given by

$$\frac{n_L}{n_{BS}} = \frac{C_L}{C_{BS} - \mathrm{IMC}} \tag{9}$$

where IMC represents the intermicellar concentration of bile salts (whose value will be seen to vary from 3 to 6 mM) in equilibrium with mixed micelles. Combining eq 8 and 9, we obtain

$$r = \frac{2\rho}{\sigma} \frac{C_L}{C_{BS} - \mathrm{IMC}} \tag{10}$$

In the limit when $C_{BS} \gg$ IMC, eq 10 implies that r should increase linearly with C_L/C_{BS}. Employing this result with the formula of Appendix A (relating r to $\bar{R}_h$), we have calculated the theoretical dependence of $\bar{R}_h$ on the L/BS ratio predicted by the Small model.[6] As shown in Figure 1, the experimental $\bar{R}_h$ values deviate markedly from the predicted dependence, particularly as the L/BS ratio approaches the phase limit. Shankland (1977) observed a similar discrepancy between the measured molecular weight of sodium cholate–lecithin mixed micelles and the predictions of the Small model, which he attributed to a stacking of the disks to form polymeric rod-shaped micelles, at ratios close to the phase limit. This hypothesis, however, is clearly incompatible with our $\bar{I}/C$ data (Figure 7) which favor a disk shape for the mixed micelles. Moreover, the suggestion that the disks polymerize is inconsistent with our observation that the $\bar{R}_h$ values increase with dilution of the total lipid concentration (Figures 3 and 4). In general, polymerized aggregates dissociate as the total concentration is diluted (Mukerjee, 1972) such as we observed in the case of primary–secondary micelle equilibrium in simple bile salt micelle solutions (Mazer et al., 1979).

Our data are, therefore, incompatible with both the Small model and Shankland's hypothesis. However, considerations based on eq 10 allow us to propose a new model of micellar structure which can account for the $\bar{R}_h$ results. Equation 10 implies that the disk radius, r, is proportional to the total amount of lecithin bilayer in the solution divided by the total amount of bile salt which is available to coat the perimeters of the disks in solutions. As the experimental disk radii are found to be much larger than those predicted by eq 10, it must be inferred that the amount of bile salt available to disperse the bilayer is actually much less than the concentration C_{BS} – IMC. This decrease in available bile salt can be accounted for in only two ways. Either (1) a significant portion of the bile salt concentration, C_{BS}, remains in solution as simple micelles or (2) the "missing" bile salts are, in fact, incorporated within the mixed micelles. If the first explanation were correct, the intermicellar concentration of bile salts should consist of a large number of simple micelles as well as bile salt monomers. However, as seen previously, the coexistence region between simple and mixed micelles is limited to low L/BS ratios, and, furthermore, our experimental deductions of the IMC values (section D) will show that the presence of simple micelles at high L/BS ratios is most unlikely. We therefore conclude that the mixed micelle must contain bile salts both

[5] In actual fact, the mixed micelles *are* polydisperse in size and composition. Equation 9, nevertheless, gives the average molar ratio of lecithin to bile salt in the mixed micelles.

[6] These calculations assume the value of $2\rho/\sigma$ to be 17.5 Å and the thickness of the micellar disk to be 50 Å.

on the perimeter of the disk and within its interior, as illustrated in Figure 11B. In this "mixed disk" model, the mixed micelle consists of a bilayer disk which contains *both* lecithin and bile salt molecules. As in the Small model, the disk is surrounded on its perimeter by a "ribbon" of bile salts. We have suggested in Figure 11B that the bile salts within the bilayer are hydrogen-bonded dimers.[7] This type of "reversed micelle" within the lipophilic environment of the lecithin has been proposed for the structure for the lamellar and cubic phases of the bile salt–lecithin–water system (Small & Bourgès, 1966; Lindblom et al., 1976). Quantitatively, however, it is important to specify how the number of bile salts contained in the interior of the disk varies with the disk radius, r. In this regard, we shall assume that the ratio of lecithin to bile salt molecules in the mixed bilayer always remains equal to the value α (where α may depend on bile salt species, temperature, and ionic strength) independent of r. Thus, if n_L and n_{BS} are the total number of lecithin and bile salt molecules in the mixed micelle and n^i_{BS}, the number of bile salts in the interior of the disk, the following relations must hold:

$$\frac{n_L}{n^i_{BS}} = \alpha \tag{11a}$$

$$n_L = \pi r^2 \sigma' \tag{11b}$$

$$n_{BS} - n^i_{BS} = 2\pi r \rho \tag{11c}$$

where σ' is the number of lecithin molecules per unit area of the mixed bilayer and ρ is the same as described before. Solving the above equations to express r in terms of n_L and n_{BS}, we obtain

$$r = \frac{\frac{2\rho}{\sigma'}\frac{n_L}{n_{BS}}}{1 - \alpha^{-1}\frac{n_L}{n_{BS}}} \tag{12}$$

Then, substituting eq 9 into eq 12, we obtain the dependence of r on the concentrations C_L and C_{BS}:

$$r = \frac{\frac{2\rho}{\sigma'}\frac{C_L}{C_{BS} - IMC}}{1 - \alpha^{-1}\frac{C_L}{C_{BS} - IMC}} \tag{13}$$

This key result offers considerable insight into many of the phenomena encountered in this paper. First, we recognize the similarity between eq 13 and eq 10. The numerator of eq 13 provides the same linear dependence on $C_L/(C_{BS} - IMC)$ predicted in the Small model, but the denominator modifies this dependence by correcting for the fact that not all the bile salts are available to form the bile salt ribbon, due to their incorporation into the lecithin bilayer. With increasing values of $C_L/(C_{BS} - IMC)$, the denominator becomes progressively smaller than unity and the r values predicted by eq 13 will progressively deviate from those given by eq 10. In fact, eq 13 predicts a divergence in r as the value of $C_L/(C_{BS} - IMC)$ approaches α. Physically, this divergence results from the incorporation of all the bile salts in the mixed bilayer, leaving no molecules left to form the bile salt ribbon. In this way, the mixed disk model *predicts* the existence of the micellar phase limit which is seen to occur when C_L and C_{BS} satisfy the equation

$$\frac{C_L}{C_{BS} - IMC} = \alpha \tag{14}$$

This result implies that the lecithin to bile salt ratio at the micellar phase limit is given by

$$\left(\frac{C_L}{C_{BS}}\right)_{\text{phase limit}} = \alpha\left(1 - \frac{IMC}{C_{BS}}\right) \tag{15}$$

It now becomes apparent from this equation why the phase limit decreases with lowering of the total lipid concentration (Carey & Small, 1978). At high total lipid concentrations, IMC/C_{BS} is $\ll 1$ and the phase limit will approximately equal α, thus providing a measure of the L/BS ratio in the mixed bilayer. However, as the total lipid concentration decreases, IMC/C_{BS} will no longer be negligible and the quantity $1 - IMC/C_{BS}$ will substantially reduce the phase limit. As a result, the divergence in r will occur at lower L/BS ratios, as was seen experimentally. In this way, the mixed-disk model also accounts for the growth of the mixed micelles with dilution of the total lipid concentration. Finally, one can explain the temperature dependence of r through the temperature dependence of the phase limit which, from eq 15, is due to the effects of temperature on the parameters α and IMC.

Although the discussion above provides qualitative support for the mixed disk model, it remains to be shown that the theoretical dependence of r on $C_L/(C_{BS} - IMC)$ given in eq 13 is consistent with our experimental deductions of $\bar{R}_h$. In order to make the comparison between theory and experiment, however, we must first know the IMC values. In fact, the IMC values for TC–L solutions can be obtained from the dependence of $\bar{R}_h$ on total lipid concentration without specific reference to the mixed disk model (see section D). The results show that the IMC values are functions of both $\bar{R}_h$ and temperature. For the purposes of testing the mixed disk model, we employ these IMC values in order to calculate the value of $C_L/(C_{BS} - IMC)$ for each of our data points. Once this is done, we can compare theory with experiment in two separate ways. First, we use the formula for disks in Appendix A to deduce the corresponding disk radii, r, from the experimental $\bar{R}_h$ values. $1/r$ is then plotted vs. $(C_{BS} - IMC)/C_L$ which, according to eq 13, should fall on a straight line given by the linear equation

$$\frac{1}{r} = \left(\frac{2\rho}{\sigma'}\right)^{-1}\left(\frac{C_{BS} - IMC}{C_L} - \alpha^{-1}\right) \tag{16}$$

From the slope and x intercept of this plot, one can then determine the parameters $2\rho/\sigma'$ and α. Parts A, B, and C of Figure 12 display plots of $1/r$ vs. $(C_{BS} - IMC)/C_L$ based on the $\bar{R}_h$ values of TC–L solutions measured at 20, 40, and 60 °C, respectively. With the exception of the results corresponding to 10 g/dL solutions near the phase limit,[8] the data

[7] Recently Zimmerer & Lindenbaum (1979) employed calorimetric methods to measure the enthalpy change associated with the solubilization of lecithin in bile salt solution. The large negative values obtained (−2 to −5 kcal/mol of lecithin) are interpreted by those authors in the context of our "mixed disk" model and are shown to be consistent with the postulated hydrogen bonding of bile salts within the interior of the mixed micelles.

[8] The anomalous behavior of the 10 g/dL solutions may be related to the high viscosity of these solutions (R. McCabe and M. C. Carey, unpublished observations) which is probably associated with strong intermicellar interactions. As a result, the $\bar{R}_h$ values obtained at 10 g/dL are apparent hydrodynamic radii which appear from Figure 12A–C to underestimate the true radii.

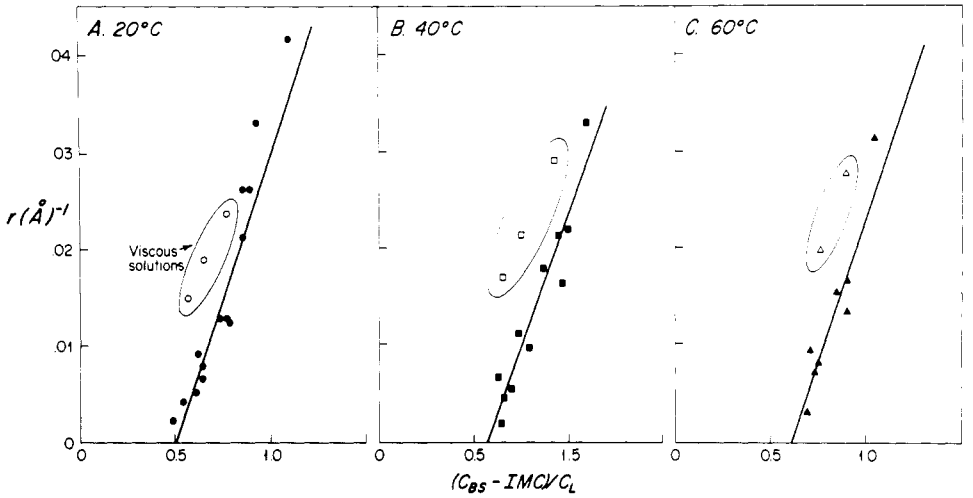

FIGURE 12: (A–C) Dependence of the disk radius r^{-1} as a function of $(C_{BS} - IMC)/C_L$ for TC–L mixed micelles at (A) 20, (B) 40, and (C) 60 °C. With the exception of the data derived in 10 g/dL viscous solutions, the data points at all other concentrations are well described by straight lines as predicted by eq 14.

Table III: Parameters Derived from Fitting the Mixed Disk Model to Experimental Data on TC–L Mixed Micelles

temp (°C)	$2\rho/\sigma'$ (Å)[a]	α[b]
20	16.66	2.0
40	18.18	1.74
60	17.03	1.64

[a] ρ equals the number of BS molecules per unit length of perimeter in the mixed micelle. σ' equals the number of lecithin molecules per unit area of mixed disk bilayer. [b] Molar ratio of lecithin to BS molecules in the mixed bilayer.

fit well to straight lines as predicted by eq 16.

Additional support for the model comes from the two parameters obtained from fitting the data with straight lines (Table III). Note that the parameter $2\rho/\sigma'$ which is derived from the slopes of the lines is roughly independent of temperature with a mean value of ~17.4 Å. We can compare this to an independent estimate of $2\rho/\sigma'$ obtained as follows. Let A_L be the area per lecithin molecule in the lamellar phase of the bile salt–lecithin system and let W represent the width of the bile salt molecule. It follows that σ' will equal $2/A_L$ and that ρ will equal $2/W$ (assuming that the bile salt "ribbon" is a close-packed structure, as depicted in Figure 11). Combining these relationships, the parameter $2\rho/\sigma'$ will be given by

$$2\rho/\sigma' = \frac{2A_L}{W} \qquad (17)$$

Substituting values for A_L (60–70 Å^2) derived from experiment (Small & Bourgès, 1966) and for W (7–9 Å) taken from molecular models (Small, 1971), one estimates from eq 17 that $2\rho/\sigma'$ should be on the order of 15–20 Å, which is in excellent agreement with our experimentally deduced value of 17.4 Å.

The α values, on the other hand, decrease with temperature, implying that fewer bile salt molecules become bound in the mixed bilayer at lower temperature. The value of $\alpha = 2.0$ obtained at 20 °C for TC–L is consistent with the maximum amount of bile salt that can be obtained in the bile salt–lecithin lamellar phase at this temperature (Small & Bourgès, 1966). In addition, is is also notable that the dependence of α on bile salt species (as inferred from the phase limits given in Figure 1) is such that α is smaller for the dihydroxy bile salts than for the trihydroxy bile salt. This suggests that the dihydroxy species are more soluble in the lecithin bilayer than the trihydroxy molecules, as would be expected from their greater hydrophobic character (Mazer et al., 1979). Thus, our deductions of $2\rho/\sigma'$ and α are each consistent with the known properties of the bile salt–lecithin system.

By use of the parameters $2\rho/\sigma'$ and α appropriate to each temperature, theory and experiment can be compared in a second way. In parts A, B, and C of Figure 13, $\bar{R}_h$ is plotted for TC–L solutions as a function of $C_L/(C_{BS} - IMC)$ at 20, 40, and 60 °C. Represented in this manner, the data points (which correspond to various total lipid concentrations and L/TC ratios, but exclude the highly viscous solutions) are seen to obey a unique functional dependence at each temperature. Moreover, the dependence obtained is in excellent agreement with the theoretical predictions based on the mixed disk model (dashed curves) but are clearly incompatible with the Small model.

In recent work, Gahwiller et al. (1977) employed QLS to measure the mean hydrodynamic radii of glycocholate (GC)–lecithin mixed micelles. Their $\bar{R}_h$ values are in excellent quantitative agreement with our own for TC and were shown in their paper to clearly deviate from the predictions of the Small model as the phase limits were approached. Gahwiller et al. (1977) attributed this discrepancy to a longitudinal polymerization of the disks (Shankland's hypothesis), a conclusion which is not supported by the present work. However, those authors did conduct further experiments that we believe provide additional support for our mixed disk model. Using spin-labeled probes (Hubbel & McConnell, 1971), differential thermal analysis (Ladbrooke et al., 1968), and fluorescence polarization of incorporated fluorophores (Schreier-Muccillo et al., 1973), their studies of mixed micelles and pure lecithin vesicles revealed (1) a lower anisotropic rotation of spin-labels in the mixed micelles relative to vesicles, (2) a broadening of the lecithin phase transition with a shift to lower temperature in mixed micelles composed of synthetic saturated lecithins, and (3) a ~65% decrease in the lateral diffusion coefficient of lipids in the mixed micelle relative to the vesicle. These effects, interestingly, are precisely the changes observed when cholesterol is incorporated in synthetic and egg lecithin bilayers (Ladbrooke et al., 1968; Galla & Sackmann, 1974; Schreier-Muccillo et al., 1973; Lippert & Peticolas, 1971) and suggest a perturbation of the lecithin environment in the mixed micelles. As the interactions between bile salts and lecithin in *monolayer* systems have been shown to exhibit similarities to those between cholesterol and lecithin (Llopis et al., 1973), it seems reasonable to assume that bile salts present in the

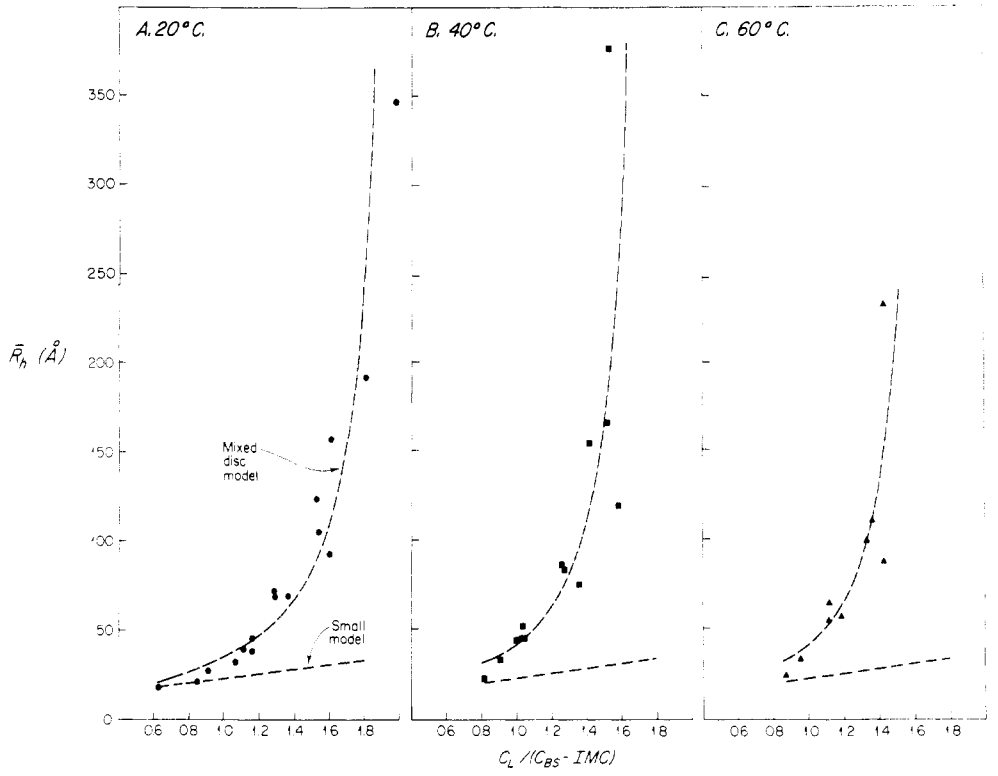

FIGURE 13: (A–C) Comparison of the experimental $\bar{R}_h$ values [plotted as a function of $C_L/(C_{BS} - IMC)$] with the theoretical dependence given by the mixed disk model and Small's model at (A) 20, (B) 40, and (C) 60 °C. Data from viscous solutions has been omitted.

mixed micelle interior could create the perturbations found by Gahwiller et al. In this regard, the 65% reduction of lipid diffusion in the mixed micelles is comparable to the reduction found in bilayers containing 30 mol % cholesterol (Galla & Sackmann, 1974) and would quantitatively support our contention that the mixed micelle contains ~33% bile salt within the lecithin bilayer.

(D) Deductions of the Intermicellar Bile Salt Concentration, IMC. In this section, deductions of the IMC are derived from a quantitative analysis of the $\bar{R}_h$ values measured at various total lipid concentrations in TC–L solutions. The analysis is based on two assumptions. The first is that the $\bar{R}_h$ value measured in the mixed micellar solution is uniquely determined by the lecithin to bile ratio within the mixed micelles (i.e., n_L/n_{BS}). Such a relationship would derive ultimately from geometric constraints on the micellar structure. From eq 9 it therefore follows that $C_L/(C_{BS} - IMC)$ must be equal to a constant $X(\bar{R}_h,T)$ for solutions having the same $\bar{R}_h$ and temperature. Second, we assume that the IMC is also dependent on $\bar{R}_h$ and T but attains the same value regardless of the concentration of the mixed micelles. This assumption would be analogous to the monomer–micelle equilibrium in simple micellar systems (Debye, 1949). Together, these two assumptions[9] imply that the concentrations (mM) of C_L and C_{BS} which produce mixed micelles of radius $\bar{R}_h$ at temperature T should satisfy the linear dependence

$$C_{BS} = \chi^{-1}(\bar{R}_h,T)C_L + IMC(\bar{R}_h,T) \qquad (18)$$

In parts A, B, and C of Figure 14 the experimental values of C_{TC} and C_L derived from TC–L solutions having the same $\bar{R}_h$ values at 20, 40, and 60 °C are shown to satisfy the linear dependence predicted in eq 18. Furthermore, by extrapolation of the straight lines fitted to each set of values, we can deduce the IMC value as a function of $\bar{R}_h$ and temperature from the y intercept of each plot. These IMC values plotted in Figure 15 decrease slightly for $\bar{R}_h$ greater than 40 Å, reaching asymptotic values of 3.2, 3.5, and 4.6 mM at 20, 40, and 60 °C, respectively. For $\bar{R}_h$ less than 40 Å, the IMC values increase abruptly, reaching ~10 mM as $\bar{R}_h$ equals 30 Å. Comparing the IMC values with the range of cmc values (Carey & Small, 1969) estimated for pure TC solutions (0.15 M NaCl) at 20, 40, and 60 °C, it is apparent that for $\bar{R}_h > 40$ Å, the bile salts present in the intermicellar solution must essentially be in a monomeric state with a concentration comparable to the cmc of the bile salt in the absence of lecithin. However, for $\bar{R}_h$ less than 40 Å, the IMC values clearly exceed the cmc and, thus, simple micelles must also be present in the intermicellar solution. This finding implies that simple micelles coexist in solutions containing the small mixed micelles and reinforces the same conclusion reached earlier from an analysis of the dependence of $\bar{R}_h$ on L/BS ratio.

The validity of the IMC values derived in this manner is supported in a number of ways. First, as was shown in Figure 4, diluting a TC–L solution with a buffer containing the IMC appropriate to the initial $\bar{R}_h$ value (taken from Figure 15) resulted in *no growth* of the mixed micelles. This can be understood as follows. If a solution of mixed micelles is diluted with an equal volume of solvent containing no bile salts, it must reestablish the IMC (which is initially reduced to half of the previous value). To do this, bile salt molecules must leave the mixed micelles, thereby increasing the ratio of lecithin to bile salt in the mixed micelles. This increase in "micellar" L/BS ratio (n_L/n_{BS}) necessitates an increase in mixed micellar size (Figure 3), consistent with our mixed disk model. However, when the diluent contains a bile salt concentration equal to the IMC, the system remains in equilibrium after dilution, thus maintaining the ratio of lecithin to bile salts in the mixed micelles and preserving $\bar{R}_h$ (Figure 4). Utilizing this principle, Shankland (1970) deduced the IMC of the cholate–lecithin

[9] These two assumptions are equivalent to those made by Shankland (1970) and Duane (1975).

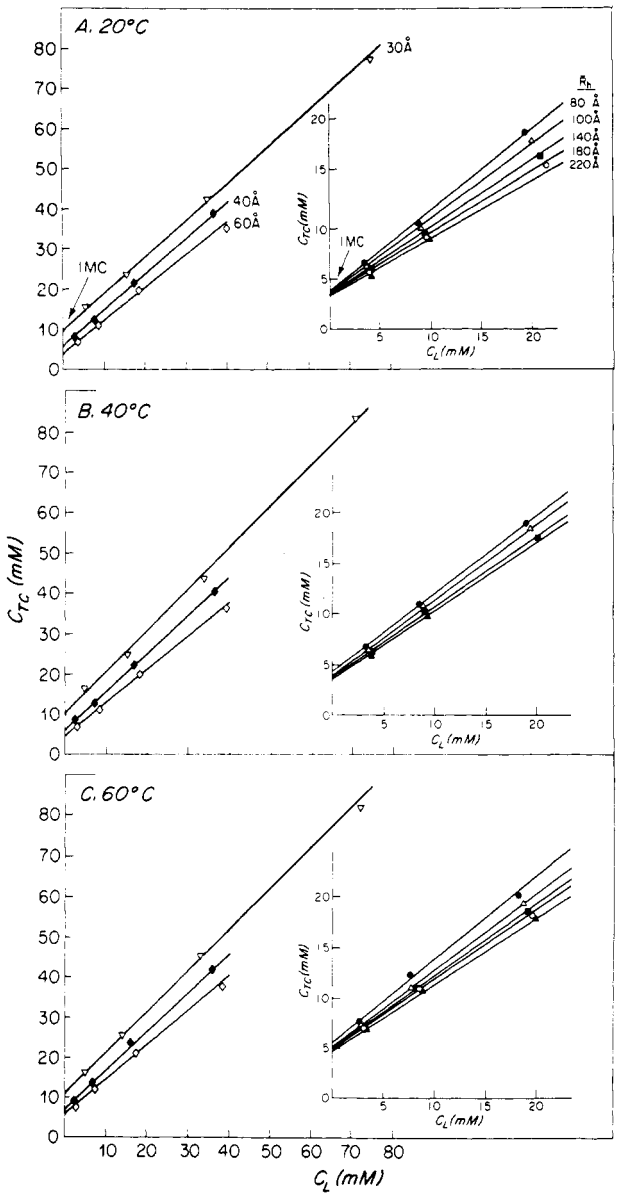

FIGURE 14: (A–C) Deductions of IMC values for TC–L solutions at (A) 20, (B) 40, and (C) 60 °C as derived from plots of C_{TC} (mM) vs. C_L (mM) corresponding to systems with the same $\bar{R}_h$ value [(▽) 30; (♦) 40; (◇) 60; (●) 80; (△) 100; (■) 140; (○) 180; (▲) 220 Å]. The linear dependence of C_{TC} on C_L is predicted by eq 18.

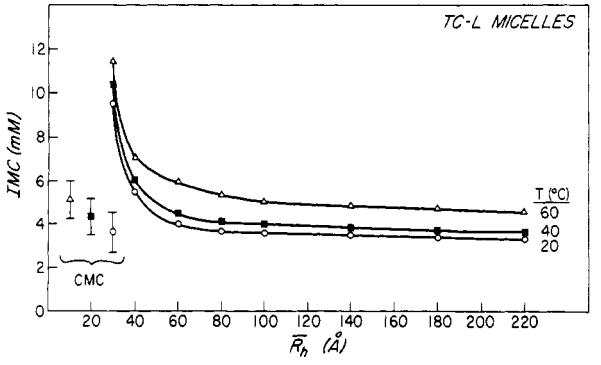

FIGURE 15: Dependence of IMC (mM) on $\bar{R}_h$ for TC–L mixed micelles at (○) 20, (■) 40, and (△) 60 °C, as derived from parts A, B, and C of Figure 14. Note also the vertical bars representing (mean ± SEM) estimates of the cmc of pure TC solutions at 20, 40, and 60 °C from Carey & Small (1969).

micelle by a trial and error method in which he identified the concentration of bile salt in the diluent which kept the apparent molecular weight of the mixed micelles constant. His values and the IMC values obtained by Duane (1975) using membrane dialysis are comparable in magnitude to the IMC values deduced in the present study. Finally, it should be noted that an estimate of the IMC can also be made directly from the micellar phase limit boundary (Figure 9) from data of Carey & Small (1978). From eq 14, it follows that the concentrations C_L and C_{BS} corresponding to the micellar phase limit should satisfy the linear equation

$$C_{BS} = \alpha^{-1} C_L + \text{IMC} \tag{19}$$

As shown in Figure 9, the experimental points of the micellar phase boundary (at 20 °C) do indeed fall on a straight line whose intercept and slope yield values of IMC = 3.2 mM and $\alpha = 1.95$. These values are in excellent agreement with the deductions obtained from the $\bar{R}_h$ data but are derived entirely from macroscopic phase equilibrium observations (Carey & Small, 1978).

Acknowledgments

The authors express thanks to Grace Ko and Jean Wu for their superb technical assistance and to Elizabeth Steeves for her excellent typing and editorial assistance. We also thank Robert Kwasnick for his assistance in conducting some of the QLS experiments. Lastly, we acknowledge the help of Elaine Lenk, Erica Hartweig, and Loretta Mengel, who performed the TEM studies.

Appendix A

Hydrodynamic Radii, Molecular Weights, and Form Factors for Rods, Disks, and Spheres. To calculate the hydrodynamic radius, $\bar{R}_h$, of rods, disks, and spheres, we employed the formula derived by R. J. Cohen (unpublished experiments), which provides an approximate method for calculating $\bar{R}_h$ for a particle of arbitrary size and shape:

$$\frac{1}{\bar{R}_h} = \frac{2}{3} V^{-1} \int_v \frac{1}{r}\, dV \tag{A1}$$

In this formula, r represents the distance from the geometric center of the particle to the volume element dV, and V is the total volume of the particle. When this equation is applied to the case of prolate and oblate ellipsoids (of which the sphere is a limiting form), it provides formulas for $\bar{R}_h$ as functions of a and b (the ellipsoidal axes) which are identical with Perrin's (1936) equations. For this reason we expect that the application of eq A1 to cylindrical and disk-shaped objects should provide good estimates of their hydrodynamic radii, for which no exact formulas yet exist. In Table AI, we list the expressions for $\bar{R}_h$ predicted for rods, disks, and spheres using eq A1. Also shown are formulas for the molecular weights, M, and scattering form factors, P (Kerker, 1969).

Appendix B

Calculation of Curve II′. The influence of micellar polydispersity was incorporated into curve II′ in the following way. Using the experimental values of $\bar{R}_h$, V, and the skewness S (if measured), we determined a two-component representation of the micellar size distribution (Mazer, 1973). The hydrodynamic radii R_1 and R_2 and the intensity ratio I_1/I_2 of these two components are related to $\bar{R}_h$, V, and S by the equations

$$R_1 = \frac{\bar{R}_h}{1 + V\left[\frac{S}{2} - \left(1 + \frac{S^2}{4}\right)^{1/2}\right]} \tag{B1}$$

Table AI[a]

shape	R_h	M^b	P
rod	$\frac{3}{4}d\left(\left[1+\left(\frac{L}{d}\right)^2\right]^{1/2}+\frac{d}{L}\ln\left[\frac{L}{d}+\left[1+\left(\frac{L}{d}\right)^2\right]^{1/2}\right]-\frac{L}{d}\right)^{-1}$	$\frac{\pi d^2}{4}L$	$P=\frac{2}{KL}\int_0^{KL}\frac{\sin\chi}{\chi}d\chi-\left[\frac{\sin(KL/2)}{KL/2}\right]^2$
disk	$\frac{3}{2}r\left(\left[1+\left(\frac{t}{2r}\right)^2\right]^{1/2}+\frac{2r}{t}\ln\left[\frac{t}{2r}+\left[1+\left(\frac{t}{2r}\right)^2\right]^{1/2}\right]-\frac{t}{2r}\right)^{-1}$	$\pi r^2 t$	$P=\frac{8}{(Kr)^2}\left[1-\frac{2}{Kr}J_1(Kr)\right]$
sphere	a	$\frac{4}{3}\pi a^3$	$P=\left[\frac{3}{(Ka)^3}[\sin(Ka)-Ka\cos(Ka)]\right]^2$

[a] L, length of rod; d, diameter of rod; r, radius of disk; t, thickness of disk; a, radius of sphere; J_1, first Bessel function; K, wave vector. [b] Density = 1.

$$R_2 = \frac{\bar{R}_h}{1 + V\left[\frac{S}{2} + \left(1 + \frac{S^2}{4}\right)^{1/2}\right]} \quad \text{(B2)}$$

$$\frac{I_1}{I_2} = \left[\frac{S}{2} + \left(1 + \frac{S^2}{4}\right)^{1/2}\right]^2 \quad \text{(B3)}$$

From curve II, we then deduced the product M_1P_1 and M_2P_2 corresponding to R_1 and R_2, respectively. The weight average of this two-component distribution is then given by

$$(MP)_w = \frac{C_1M_1P_1 + C_2M_2P_2}{C_1 + C_2} \quad \text{(B4)}$$

which is equivalent to

$$(MP)_w = \frac{(C_1/C_2)M_1P_1 + M_2P_2}{C_1/C_2 + 1} \quad \text{(B5)}$$

where C_1/C_2 is the ratio of concentrations (w/v) of species 1 and 2. This ratio, however, can be deduced experimentally from I_1/I_2 by using the relation

$$\frac{I_1}{I_2} = \frac{C_1M_1P_1}{C_2M_2P_2} \quad \text{(B6)}$$

Thus, given the values $\bar{R}_h$, V, and S, one can determine M_1P_1, M_2P_2, and C_1/C_2 and thereby use eq B5 to calculate $(MP)_w$.

Appendix C

Calculation of the V Values in the Coexistence Region. The V value obtained from QLS is related (Mazer et al., 1976a, 1979) to the first and second moments of the distribution of micellar diffusion coefficients $\bar{D}$ and $\overline{D^2}$ as seen in eq C1:

$$V = 100(\overline{D^2} - \bar{D}^2)^{1/2}/\bar{D} \quad \text{(C1)}$$

In a system containing both simple and mixed micelles, it can be shown that the values of $\bar{D}$ and $\overline{D^2}$ for the entire distribution of micellar species will be given by

$$\bar{D} = \left(\bar{D}_s + \frac{I_m}{I_s}\bar{D}_m\right)\Big/\left(1 + \frac{I_m}{I_s}\right) \quad \text{(C2)}$$

$$\overline{D^2} = \left[\overline{D^2}_s + \frac{I_m}{I_s}\overline{D^2}_m\right]\Big/\left(1 + \frac{I_m}{I_s}\right) \quad \text{(C3)}$$

where the subscripts "s" and "m" correspond to values obtained in pure solutions of simple and mixed micelles, respectively, and I_m/I_s is the ratio of intensities scattered by simple and mixed micelles in a solution where both species coexist.

The values of $\overline{D^2}_s$ and $\overline{D^2}_m$ can be determined experimentally from the variances V_s and V_m by the following relations which are based on eq C1:

$$\overline{D^2}_s = \left(\frac{V_s\bar{D}_s}{100}\right)^2 + \bar{D}^2_s \quad \text{(C4)}$$

$$\overline{D^2}_m = \left(\frac{V_m\bar{D}_m}{100}\right)^2 + \bar{D}^2_m \quad \text{(C5)}$$

Thus, from $\bar{D}_s$, $\bar{D}_m$, V_s, and V_m, one can derive $\bar{D}$ and $\overline{D^2}$ corresponding to the distribution of simple and mixed micelles, as a function of I_m/I_s. Then, by use of eq C1, the V value can be calculated.

Appendix D

Calculations of the $\bar{R}_h$ Values in TDC–L Solutions in 0.6 M NaCl. As in the case of the TC–L system, the basic equations for calculating $\bar{R}_h$ in the coexistence region remain eq 2 and 3. The essential difference, however, in the TDC–L solutions is that the values of $\bar{R}_s$ and $\bar{M}_s$ are now functions of C_s and temperature in accordance with the model of primary–secondary micelle equilibrium given in our earlier paper (Mazer et al., 1979). This model showed that $\bar{R}_s$ and $\bar{M}_s$ depend only on the product of the polymerization constant K (which is a function of temperature) and the concentration C_s. In calculating the $\bar{R}_h$ values of Figure 10, we have thus employed eq 2 and 3 in conjunction with values of $\bar{R}_s$ and $\bar{M}_s$ which were predicted from this model, using the experimentally determined values of $K(T)$ obtained previously (Mazer et al., 1979).

References

Carey, M. C., & Small, D. M. (1969) *J. Colloid Interface Sci. 31*, 382.

Carey, M. C., & Small, D. M. (1970) *Am. J. Med. 49*, 590.

Carey, M. C., & Small, D. M. (1978) *J. Clin. Invest. 61*, 998.

Cohen, R. J., Jedziniak, J. A., & Benedek, G. B. (1976) *J. Mol. Biol. 108*, 179.

Debye, P. (1949) *Ann. N.Y. Acad. Sci. 51*, 575.

Duane, W. (1975) *Biochim. Biophys. Acta 398*, 275.

Gahwiller, C., von Planta, C., Schmidt, D., & Steffen, H. (1977) *Z. Naturforsch. C 32*, 748.

Galla, H., & Sackmann, E. (1974) *Biochim. Biophys. Acta 339*, 103.

Hall, C. E. (1953) *Introduction to Electron Microscopy*, pp 318–323, McGraw-Hill, New York.

Hubbel, W. L., & McConnell, H. M. (1971) *J. Am. Chem. Soc. 93*, 314.

Kerker, M. (1969) *The Scattering of Light and Other Electromagnetic Radiation*, Academic Press, New York.

Koppel, D. E. (1972) *J. Chem. Phys. 57*, 4814.

Ladbrooke, B. D., Williams, R. M., & Chapman, D. (1968) *Biochim. Biophys. Acta 150*, 333.

Lindblom, G., Winnerstrom, H., Arvidson, G., & Lindman,

B. (1976) *Biophys. J. 16*, 1287.
Lippert, J. L., & Peticolas, W. L. (1971) *Proc. Natl. Acad. Sci. U.S.A. 68*, 1572.
Llopis, J., Albert, A., Saiz, J. L., & Alonso, D. (1973) *Chemistry, Physical Chemistry and Applications of Surface Active Substances*, Vol. 2, pp 339–349, Carl Hauser and Verlag, Munich.
Mazer, N. A. (1973) S.B. Thesis, Massachusetts Institute of Technology.
Mazer, N. A. (1978) Ph.D. Thesis, Massachusetts Institute of Technology.
Mazer, N. A., Benedek, G. B., & Carey, M. C. (1976a) *J. Phys. Chem. 80*, 1075.
Mazer, N. A., Benedek, G. B., & Carey, M. C. (1976b) *Gastroenterology 70*, 998.
Mazer, N. A., Carey, M. C., & Benedek, G. B. (1977) in *Micellization, Solubilization and Microemulsions* (Mittal, K. L., Ed.) Vol. 1, pp 359–381, 383–402, Plenum Press, New York.
Mazer, N. A., Carey, M. C., Kwasnick, R., & Benedek, G. B. (1979) *Biochemistry 18*, 3064.
Montet, J. C., & Dervichian, D. G. (1971) *Biochimie 53*, 751.
Mukerjee, P. (1972) *J. Phys. Chem. 76*, 565.
Perrin, R. (1936) *J. Phys. Radium 7* (*7*), 1.
Schreier-Muccillo, S., Marsh, D., Dugas, H., Schneider, H., & Smith, I. C. P. (1973) *Chem. Phys. Lipids 10*, 11.
Shankland, W. (1970) *Chem. Phys. Lipids 4*, 109.
Shankland, W. (1977) *Chem. Phys. Lipids 19*, 20.
Small, D. M. (1967a) *Gastroenterology 52*, 607.
Small, D. M. (1967b) *J. Lipid Res. 8*, 551.
Small, D. M. (1971) in *The Bile Acids* (Nair, P. P., & Kritchevsky, D., Eds.) Vol. 1, pp 249–355, Plenum Press, New York.
Small, D. M., & Bourgês, M. (1966) *Mol. Cryst. 1*, 541.
Small, D. M., Penkett, S. A., & Chapman, D. (1969) *Biochim. Biophys. Acta 176*, 178.
Tausk, R. J. M., Karmiggett, J., Oudshoorn, C., & Overbeek, J. Th. G. (1974) *Biophys. Chem. 1*, 175.
Zimmerer, R., & Lindenbaum, S. (1979) *J. Pharm. Sci. 68*, 58.

Hydrolysis of Di- and Trisialo Gangliosides in Micellar and Liposomal Dispersion by Bacterial Neuraminidases†

Benvenuto Cestaro,‡ Yechezkel Barenholz, and Shimon Gatt*

ABSTRACT: The hydrolysis of di- and trisialo gangliosides by bacterial neuraminidases was investigated. Slow rates of hydrolysis were obtained with micellar dispersions of the pure gangliosides; the rates increased considerably with mixtures of ganglioside and phospholipids, such as phosphatidylcholine or sphingomyelin. The greatest rates of hydrolysis were obtained with mixtures containing 5–10 mol % ganglioside and 90–95% phospholipid. With the aid of the nonpenetrating reagent trinitrobenzenesulfonic acid, it was ascertained that this mixture consisted of sealed, unilamellar vesicles in which the ganglioside was distributed symmetrically between the two layers of the liposome. When the relative proportion of the ganglioside was increased, the dispersions contained liposomes admixed with micelles of ganglioside and phospholipid. The rates of hydrolysis of the ganglioside could be correlated with the percentage of sealed vesicles in each mixture. Experiments in which another ganglioside (GM1) or cholesterol was incorporated into the mixed dispersions further supported this conclusion. It is suggested that the rate of hydrolysis is affected predominantly by interactions between the carbohydrate chains of ganglioside molecules. The data emphasize that ganglioside metabolism can be best studied when the latter are part of biological or model membranes.

Gangliosides are glycosphingolipids which contain one or more residues of sialic *N*-acetylneuraminic acid. They are minor components of plasma membranes of many vertebrate cells. Their contribution to the physical and biological properties of the membranes is mainly due to the negative charge of the sialic acid and their large carbohydrate head group. Although their precise biological role has not been established, they were shown to be receptors of bacterial toxins, viruses, hormones, and interferon, and their compositional pattern in cell surface changes drastically following transformation [for a review see Yamakawa & Nagai (1978), Klenk (1973), Wallach (1975), Fishman & Brady (1976), Svennerholm & Mandel (1979), Klenk & Huang (1973), Fishman et al. (1973), Hakomori (1973), and Murray et al. (1973)]. It has been proposed that they might act as chelators for calcium and possibly other divalent ions (Harris & Thornton, 1978).

Hydrolysis of sialyl residues by neuramidases is the key step in ganglioside catabolism (Gatt, 1970). Neuraminidase action reduces the number of NANA residues, thereby affecting their physical and biological activities.

Several mammalian neuraminidases have been described in various subcellular localization including those of plasma membrane, lysomal membrane, synaptic membrane, and a soluble enzyme from the cytosol; some enveloped viruses also have neuraminidase in their membrane [for a review see Dawson (1978), Tettamanti et al. (1978), Rosenberg (1978), Veh & Schauer (1978), Sandhoff et al. (1978), and Venerando (1978)].

Experimental Procedure

Materials and Enzymes. Gangliosides were purified by G. Tettamanti using previously described procedures (Tettamanti

† From the Laboratory of Neurochemistry, Department of Biochemistry, Hebrew University–Hadassah Medical School, Jerusalem, Israel. *Received February 7, 1979.* Supported in part by National Institutes of Health Grant NS02967 and United States–Israel Binational Science Foundation Grant 1688/78.
‡ CNR Fellow. Permanent address: Institute of Biological Chemistry, Faculty of Medicine, University of Milano, Milano, Italy.

0006-2960/80/0419-0615$01.00/0